Theor Chem Acc (2000) 105:145–155
DOI 10.1007/s002140000192

Theoretical
Chemistry Accounts

Original article

Following the streambed reaction on potential-energy surfaces: a new robust method

Wolfgang Quapp[1], **Michael Hirsch**[1], **Dietmar Heidrich**[2]

[1] Mathematisches Institut, Universität Leipzig, Augustus-Platz, 04109 Leipzig, Germany
[2] Wilhelm-Ostwald-Institut für Physikalische und Theoretische Chemie, Universität Leipzig, Linnéstr.2, 04103 Leipzig, Germany

Received: 8 March 2000 / Accepted: 17 July 2000 / Published online: 24 October 2000

Abstract. A simple procedure with low computational efforts is proposed to follow the reaction path of the potential-energy hypersurface (PES) starting from minima or saddle points. The method uses a modification of the so-called "following the reduced gradient" [Quapp W, Hirsch M, Imig O, Heidrich D (1998) *J Comput Chem* 19:1087]. The original method connects points where the gradient has a constant direction. In the present article the procedure is replaced by taking iterative varying directions of the gradient controlled by the last tangent of the searched curve. The resulting minimum energy path is that valley floor gradient extremal (GE) which belongs to the smallest (absolute) eigenvalue of the Hessian and, hence, that GE which usually leads along the streambed of a chemical reaction. The new method avoids third derivatives of the PES and obtains the GE of least ascent by second-order calculations only. Nevertheless, we are able to follow the streambed GE uphill or downhill. We can connect a minimum with its saddles if the streambed leads up to a saddle, or we find a turning point or a bifurcation point. The effectiveness and the characteristic properties of the new algorithm are demonstrated by using polynomial test surfaces, an ab initio PES of H_2O, and the analytic potentials of Lennard-Jones (LJ) clusters. By tracing the streambeds we located previously identified saddle points for LJ_N with $N = 3$, 7, 8, and 55. Saddles for LJ_N with $N = 15$, 20, and 30 as presented here are new results.

Key words: Potential-energy surface – Reaction-path following – Saddle point – Reduced gradient – Gradient extremal

Correspondence to: W. Quapp
e-mail: quapp@server1.rz.uni-leipzig.de;
Tel.: +49-341-9732153; Fax: +49-341-9732199

1 Introduction

The concept of the minimum energy path (MEP) or reaction path of a potential-energy surface (PES) is the usual approach to theoretical kinetics of larger chemical systems [1–3]. It is able to describe pathways of conformational rearrangements as well. The reaction path is defined as the line in the configuration space which connects the reactant and the product minimum by passing the saddle point (SP) of the PES. The SP (the transition structure) and the minima form stationary points of the PES. The mathematical description of a MEP turned out to be more difficult than expected [4]. Any algorithm which allows this pathway to be determined in a suitable approximation should be tested. Especially the search for valley pathways is an important part of the PES analysis which still offers no satisfactory concept. This search is not equivalent to the finding of steepest descent pathways, which, of course, are simpler to calculate. The usual "reduced gradient following" (RGF) curves (see later) can only be used in certain cases [5, 6]; however, a simple and exact valley-floor characterization of a reaction channel is a prerequisite for a number of dynamical theories to come into operation, including the famous reaction path Hamiltonian [2]. Further, the variational transition state theory [3, 7] needs an exact description of the reaction path [8]. It is of particular interest that the knowledge of the reaction pathways may give tools for the interpretation of IR spectra of vibrationally highly excited molecules [9] and for the study of mode-selective reactions.

The gradient extremal [10–14] (GE) appeared to represent a suitable ansatz for a MEP, but, with its manifold of curves and turning points, this concept in its general form is not suitable for use as a routine program for the calculation of reaction paths; for an example of systematic use see Ref. [15]. The combination of the GE concept with the RGF [5, 6] presented here provides a manageable way to follow the streambed of the PES. The term "streambed leading to a minimum" is used to characterize the reaction path in understandable two-dimensional model surfaces [17], but it is used

synonymously in any dimension. Mathematically, we understand the term streambed as the valley-floor GE of the PES following the first normal mode to the smallest (absolute) eigenvalue. This GE leaves the minimum with the gentlest ascent.

The RGF finds a curve where the selected gradient direction comes out at every curve point, $\mathbf{x} = \mathbf{x}(t)$:

$$\nabla E[\mathbf{x}(t)]/||\nabla E[\mathbf{x}(t)]|| = \mathbf{r} \ , \tag{1}$$

where t is the curve parameter and $\mathbf{r}$ is the unit vector of the fixed search direction [6]. The RGF method needs gradient and (updates of) the Hessian of the PES. There are curves which pass all stationary points of the PES. Thus, the RGF is a simple but effective procedure in order to determine all types of stationary points [5]. Unlike the steepest descent path from a saddle, the reduced gradient search for a fixed direction locally has an explicit analytical definition. In other words, the difference between the two kinds of curves is that the RGF does not give a curve through every point. We recall that the RGF curves are not generally MEPs. Nevertheless, these curves may follow a reaction path in favorable cases, at least qualitatively.

The idea behind this work is to modify the RGF method to intrinsically search the MEP. We formally replace the constant search direction, $\mathbf{r}$, in Eq. (1) of the RGF method by a variable direction. We take the tangent of the searched curve itself as new gradient direction. This may sound like a vicious circle; however, it is iteratively realizable because the RGF method is separated into predictor and corrector steps. Every corrector step is calculated with the tangent direction of the previous predictor. Quickly, this leads to self-consistency on the valley-floor GE. We term the method the tangent search correction to the RGF method, or shorter the tangent search concept (TASC). (The task is to find the MEP!) Practically, Eq. (1) is realized by a projector ansatz [6] (see later) and the curve-following requires the derivation of the ansatz. However, we do not derive the projector of the "reduced gradient" to calculate the tangent of the next predictor. With this trick we avoid the irritating third derivatives of the PES which occur in the terms of current GE calculations [13–15]. We have to use nonredundant internal coordinates to avoid problems resulting from the so-called zero eigenvalues of the translational or rotational motion of the chemical system (see Refs. [9, 16] for a short description). Then, usually the smallest absolute eigenvalue of the Hessian belongs to that eigenvector which describes the streambed direction of the reactive well. A counterexample is the Don Quixote type SP [18] (a SP with a large negative and a small positive force constant, as one might use on an emaciated horse (see later for a discussion). Our TASC is strictly limited to following the direction of the smallest eigenvalue; however, the new method is very robust and also works in cases where turning points of the streambed GE appear (in a region where valleys disappear). Such regions are overcome by successive corrector steps. With the new TASC in connection with the RGF we propose a practicable algorithm for the main part of chemical reaction pathways.

The article is organized as follows. First, we briefly repeat the mathematical fundamentals of the RGF method [5, 6, 9] and define the modified RGF by the iterative method of the "tangent search". Subsequently, the success is demonstrated by some examples, including an ab initio PES of the water molecule. We show with the help of a test potential the success of the TASC to overcome turning points of the valley-floor GE. In a counterexample we show that a SP lying beside the "lowest" streambed is not accessible by the TASC. (To find the SP, the TASC has to be combined with the original RGF.) In a further test, we compute the isomerization valleys and the corresponding SPs of Lennard-Jones (LJ) clusters with from three up to 55 particles. In the Appendix we present the scheme of the algorithm and we prove that the TASC is equivalent to the GE equation. The method is implemented as a subroutine in our research code of the GAMESS-UK program [19], which is available on request.

2 Modification of the RGF by following the tangent of the previous predictor step: TASC

$E(\mathrm{x})$ is the function of the PES and $\nabla E(\mathbf{x})$ is its gradient vector, $\mathbf{g}(\mathbf{x})$, in the configuration space, $\mathbf{R}^{\mathrm{n}}$, defined by the coordinates x of the molecule where, as usual, $n = 3N - 6$ is the number of independent internal coordinates forming the dimension of the problem. $\mathbf{x}$ and $\mathbf{g}$ are vectors of the dimension n. To realize the requirement (Eq. 1), the RGF algorithm [6] uses a projection of the gradient of the PES to fulfill the $n - 1$ equations

$$\mathbf{P}_{\mathrm{r}}\mathbf{g}[\mathbf{x}(t)] = 0 \ . \tag{2}$$

This results in the $(n - 1)$-dimensional zero vector of the reduced gradient. The projector, $\mathbf{P}_{\mathrm{r}}$, was chosen here to be a constant $(n - 1) \times n$ matrix: that one which forces the gradient to point at every curve point, $\mathbf{x}(t)$, in the same direction, $\mathbf{r}$. The tangent to this curve, $\mathbf{x}'(t)$, is obtained by the solution of the following system of equations:

$$\frac{\mathrm{d}}{\mathrm{d}t}\{\mathbf{P}_{\mathrm{r}}\mathbf{g}[\mathbf{x}(t)]\} = \mathbf{P}_{\mathrm{r}}\frac{\mathrm{d}\mathbf{g}[\mathbf{x}(t)]}{\mathrm{d}t} = \mathbf{P}_{\mathrm{r}}\mathbf{H}[\mathbf{x}(t)]\mathbf{x}'(t) = 0 \ , \tag{3}$$

where $\mathbf{H}$ is the Hessian of the PES. The simplicity of the RGF method is based on the constancy of the $\mathbf{P}_{\mathrm{r}}$ matrix. Now, we allow the projector to change after the predictor step: the tangent direction of the previous curve point iteratively becomes the search direction for the next point of the curve. The procedure is named the TASC. (A computational scheme is given in the Appendix.) All the calculations of the predictor–corrector method where done using Eqs. (2) and (3). In the derivation of Eq. (3) we further assume a "constant" $\mathbf{P}_{\mathrm{x}'}(t)$ matrix in the current step. This is an approximation, but it works well and accelerates the calculation of the streambed line. If necessary, the TASC changes the corresponding RGF curve after the predictor step. Figure 1 illustrates the action of the TASC by a schematic sketch with the test potential

$$E(x, y) = 2x^3 + 6\left(xy^2 - x^2 + y^2\right) \ . \tag{4}$$

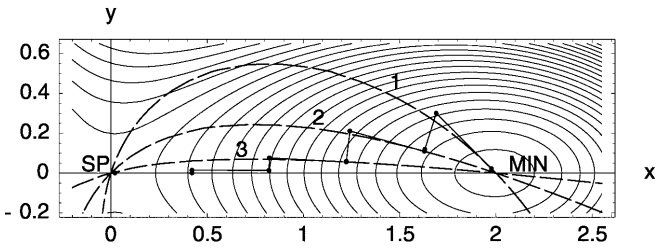

Fig. 1. Action of the tangent search concept (*TASC*) on a model potential [5]: the points are calculated with fixed predictor steps of 0.4 and a corrector tolerance of 0.001. *Curve 1* is the solution of the reduced gradient following (*RGF*) to direction (−1, 3). This is also the start direction of the TASC. *Curves 2* and *3* are the corresponding RGF solutions to the tangent directions of the TASC point of the preceding curve. The streambed gradient extremal (*GE*) is the *x*-axis. (There are five predictor steps to the saddle point, *SP*.)

To make things visible, the starting point at (1.977, 0.022) is chosen near the minimum, and the start direction of the gradient searched is chosen to be (−1, 3). Thus, we selected the initial direction somewhat skew to the searched MEP along the *x*-axis. Additionally, we took a large step length of 0.4 for the predictor, but a low threshold of 0.001 for the corrector steps. The first projector is the orthogonal vector to the first search direction: (0.948, 0.316). It is applied to the Hessian matrix

$$\mathbf{H}(1.977, 0.022) = \begin{pmatrix} 11.726 & 0.270 \\ 0.270 & 35.726 \end{pmatrix} \ , \tag{5}$$

giving the reduced equation $11.210x' + 11.553y' = 0$. The tangent vector is (−0.718, 0.696); the first predictor step is (−0.288, 0.279). Curve 1 is the RGF curve which follows the start direction. The first predictor step of the TASC goes along with curve 1; however, corrector steps do not stop at this curve because of considering the new direction (−1, 0.97) of the tangent at the starting point. The next projector is (0.696, 0.718). The corresponding corrector step is (−0.059, −0.182). It is evident that the corrector exactly converges to curve 2, which is the RGF solution to this second direction. Again, at every point of curve 2, the gradient has this direction (−1, 0.97), but now the tangent at the TASC point at curve 2 has again turned to another direction (−1, 0.26), and the next corrector steps have to search the new curve 3, and so on. The points calculated by the TASC are the following:

S (1.977, 0.022),		
P (1.690, 0.301),	C (1.631, 0.119),	C (1.628, 0.110),
P (1.241, 0.211),	C (1.223, 0.059),	C (1.223, 0.056),
P (0.824, 0.076),	C (0.821, 0.014),	
P (0.421, 0.016),	C (0.421, 0.0006),	
P (0.021, 0.0003),		

where S is the start, P are predictor steps, and C are corrector steps.

In general, the resulting curve meets the valley floor after some steps. This is nearly independent of the chosen initial direction: after a small number of steps, the method follows the streambed of the valley along the direction of the eigenvector with the smallest (absolute) eigenvalue. In the Appendix, we prove that the GE equation is actually the background of the TASC, and the resulting curve is a numeric approximation of the valley-floor GE. The reason for this nice behavior is an intrinsic action of the RGF method. This can be explained using the equivalent differential equation of Branin [20], which has the same solution curve as the RGF method [6]. It is

$$\frac{\mathrm{d}\mathbf{x}}{\mathrm{d}t} = \mathbf{x}'(t) = \pm \mathbf{A}\ \mathbf{g}[\mathbf{x}(t)] \ , \tag{6}$$

where $\mathbf{x}'(t)$ is the tangent to the solution curve of the RGF ansatz, and **A** is the adjoint matrix of the Hessian. **A** is defined by $\mathbf{AH} = \det(\mathbf{H})\mathbf{I}$, with the unit matrix, **I**. If $\mathbf{e}_1, \ldots, \mathbf{e}_n$ are the eigenvectors of **H** with eigenvalues $\lambda_1, \ldots, \lambda_n$ then they are also the eigenvectors of **A** but with the eigenvalues $\mu_1 = \lambda_2\lambda_3 \cdots \lambda_n, \ \ldots,$ and $\mu_n = \lambda_1\lambda_2 \cdots \lambda_{n-1}$. This is due to the equation

$$\mathbf{H}\mathbf{e}_i = \lambda_i \mathbf{e}_i \tag{7}$$

and by multiplication with the adjoint matrix we get

$$\mathbf{AH}\ \mathbf{e}_i = \det(\mathbf{H})\mathbf{e}_i = \lambda_i \mathbf{A}\mathbf{e}_i \ , \tag{8}$$

with

$$\det(\mathbf{H}) = \prod_{k=1}^{n} \lambda_k \ . \tag{9}$$

If a point of the solution curve of the RGF method with the search direction **r** is reached the gradient of Eq. (6) points in the same direction. Expressing **r** by the eigenvectors

$$\mathbf{r} = \sum_{i=1}^{n} \mathrm{r}_i\ \mathbf{e}_i \tag{10}$$

we obtain the relation for the tangent direction

$$\mathbf{x}' = \mathbf{A}\mathbf{r} = \sum_{i=1}^{n} r_i \det(\mathbf{H})/\lambda_i\ \mathbf{e}_i \ . \tag{11}$$

If λ_1 is the smallest (absolute) eigenvalue then the $\mathbf{e}_1$ component of the preceding search direction **r** is enforced if in the next step the new direction $\mathbf{x}'$ (Eq. 11) is used in Eqs. (2) and (3). Thus, if the search direction is the tangent of an RGF curve, this direction is now turned to the $\mathbf{e}_1$ direction. The action is larger the larger the differences of the eigenvalues $\lambda_2, \ldots, \lambda_n$ are against λ_1. Only for $r_1 = 0$ does this action of eigenvector weighting not work (e.g., if the direction $\mathbf{e}_1$ is orthogonal to a symmetry plane where the TASC searches). Equation (11) allows an effective procedure of eigenvector-following to the smallest eigenvalue, λ_1. Using the TASC, the diagonalization of the Hessian to calculate the eigenvectors is not necessary. The aspect becomes computationally important for very large systems [21]. In contrast to the well-known method of eigenvector-following [22–24], our method provides a locally defined curve, found by a predictor–corrector scheme as used in Ref. [5] for the RGF method. So we can calculate this pathway as exactly as necessary, if we diminish the step length of the predictor and the threshold of the corrector.

3 Success of the TASC

3.1 Example H_2O: GE along the bending mode

The restricted Hartree–Fock method using the 3-21 Gaussian basis set (RHF/3-21G) is applied to follow the reaction path of dissociation in the water molecule. It is obvious that the simple quantum chemical level used is not sufficient to give a globally correct PES of H_2O. Especially, dissociations such as $H_2O \rightarrow O + H_2$ cannot be described adequately without using the complete-active-space self-consistent-field method or related methods. It is not the objective of this article to give an exact description of the high-energy parts of the water PES. In contrast, the ab initio PES is only used as a model surface. The pathway of interest starts from the minimum and goes uphill following the eigenvector direction of the bending mode. The PES analysis is illustrated in Fig. 2 by using the symmetric surface section [9]. The axes are the symmetric OH distances (in angstroms) and the bending angle of the bonds. In the curvilinear internal coordinates, the scaling of 0.1 Å is equivalent to an angle of about 5.7°. The curve obtained by the TASC is depicted by dots. The two pathways uphill starting at the minimum and the corresponding pathways downhill (starting at the SP at 180° and the "dissociation channel" near 30°, respectively) are the same curves. We may interpret the curves to be numeric reaction path approximations. They correspond to the valley-floor GE of the smallest eigenvalue. This may be illustrated by the σ surface of the water molecule shown in Fig. 2 by thin equi-σ lines. The measure for the ascent of the PES functional, $E(\mathbf{x})$, is the norm of the gradient vector $\mathbf{g}=(g_1,...,g_n)$. A point showing the gentlest ascent of a valley is defined by the condition that the norm-quadrat of the gradient,

$$\sigma(\mathbf{x}) = \frac{1}{2}||\mathbf{g}(\mathbf{x})||^2 \ , \tag{12}$$

forms a minimum taken along an equipotential surface, $E(\mathbf{x}) = \text{constant}$, i.e., along all directions perpendicular to the gradient, $\mathbf{g}$ [10, 11, 25]. In other words, the projection of $\nabla\sigma(\mathbf{x})$ onto all directions orthogonal to the gradient vanishes [11]. If $\sigma(\mathbf{x})$ has a minimum then the PES has the gentlest ascent, and, therefore, we have a streambed GE, a "GE channel" [17], provided that the curvature orthogonal to the ascent direction shows the features of a valley. In Fig. 2 we see that the dotted curve connects those points where the equilines of both surfaces (PES and σ surface) have the same tangents. This is the proof that the dotted curve is actually the GE of the PES. This streambed GE is here qualitatively comparable with the steepest descent from the SP, the intrinsic reaction coordinate (IRC).

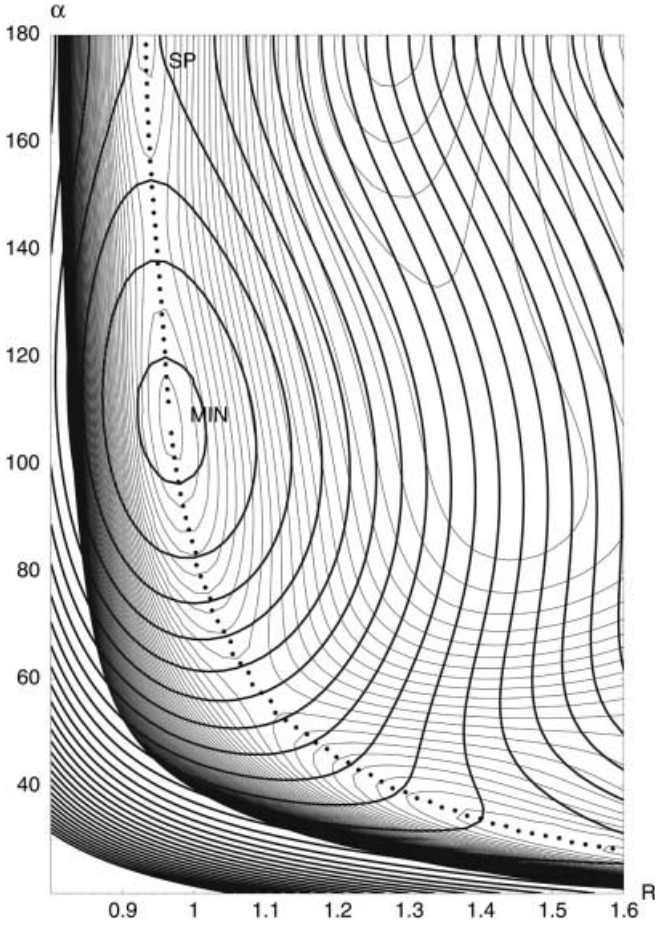

Fig. 2. Restricted Hartree-Fock/3-21G potential surface of the water molecule in the symmetric section. The *bold lines* are the equipotential lines, the *underlying thin lines* are the equi-σ lines. GEs should connect those points where both systems of equipotential lines come into contact. The *dotted line* from the SP at 180° to the minimum (*MIN*) and again uphill to the "dissociation channel" near 30° is the streambed GE found using the TASC

3.2 Turning points of streambed GEs and the disappearance of a valley

Turning points can emerge along a streambed GE which correctly describes the supposed valley-floor path. They indicate the disappearance of the valley. However, it is possible that a new valley is formed in the neighborhood. In this case, the GE wanders about the surface rather than taking the most direct route to the transition structure. The situation is illustrated by a simple polynomial test surface. The example [26] of Fig. 3 is

$$\begin{aligned} E(x,y,z) = {} & a\left(x^2-1\right)^2 + 16y^2(y-b)^2 + 10z^2 \\ & + [y-c(x+1)]^2[y+b(x-1)]^2 + [y+c(x-1)]^2 \\ & \times [y-b(x+1)]^2 \ , \end{aligned} \tag{13}$$

where $a=0.1553$, $b=0.5$, and $c=-0.7$. The z coordinate may simulate the $(n-2)$ remaining coordinates of a molecule; it is only symbolically given by a strong pure harmonic term. We find in the (x, y) plane at $z=0$ an "uphill streambed" starting at the minimum (−1, 0) and climbing up to the turning point TP_1 at about (−0.57, 0.06). Here, the valley disappears at the slope of the PES: this happens at the turning point of the valley-floor GE. In addition, we also have a "downhill streambed" GE

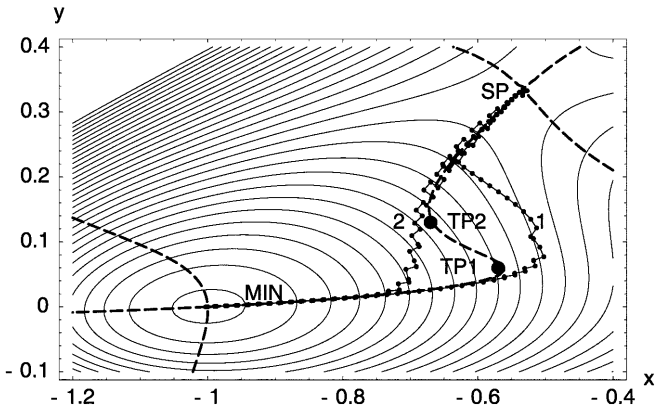

Fig. 3. Model potential surface [26], $E(x, y, z) = a(x^2 - 1)^2 + 16y^2(y - b)^2 + 10z^2 + [y - c(x + 1)]^2[y + b(x - 1)]^2 + [y + c(x - 1)]^2[y - b(x + 1)]^2$, with a MIN and a SP at the $z = 0$ section. Analytically calculated GEs are shown by *bold dashed lines*. The tangent search (TASC, *dotted connected curve*) explores the two pieces of the streambed GE between the left minimum and the SP (*curve 1*). These parts are disturbed by two turning points. The turning point region is passed by corrector steps. The same is valid for the downward search (*curve 2*)

from the SP at (−0.53, 0.33) downwards to the turning point TP_2 at about (−0.67, 0.12). The connection between the two turning points is also described by the solution of the GE equation but this is not a valley floor. Thus, from a chemical standpoint it is not very interesting to describe this part of the GE curve in detail. The proposed TASC has the nice feature of self-correction towards the streambed GE. What happens at a turning point where the streambed ends? There, the tangent of the GE is orthogonal to the gradient. But the TASC searches a curve where the gradient points into the tangent direction of the previous RGF curve. Thus, the TASC cannot find the exact location of the turning point of the GE. (If the step length is decreased, the TASC may come nearer to this TP.) If the algorithm reaches the turning-point region, say TP_1 uphill, it "realizes", after an overshooting iteration step, the end of the TASC path. This depends on the chosen accuracy condition of the RGF equation, simply because the corrector does not converge to a curve point, owing to the absence of a further solution of the TASC behind the turning point. However, the corrector continues to work having in store the tangent of the last "unsuccessful" predictor step (we control the step length – this is necessary in contrast to the RGF) and "curve" 1 usually passes the region between the two turning points: After a more or less longer pathway it converges to the next streambed represented by the GE curve. This is the part between TP_2 and the SP, and the predictor leads the curve along the GE up to the SP. The path after a TP searched by pure corrector steps may be monitored by a simple count of the corrector steps.

Vice versa, starting in Fig. 3 at the SP and going downwards, the algorithm leads the curve along the GE down to TP_2, and there it again realizes the disappearance of the valley. The corrector searches further along "curve" 2, and at least it will converge to the lower valley-floor GE, finally finding the minimum. Note that the other eigenvalues (absolute) are throughout larger than the eigenvalue of the streambed GE. We understand the two parts between the minimum and TP_1, or between the SP and TP_2, as reaction pathways. However, the region between TP_1 and TP_2 is an "unstable" part. It is characterized by the change from the terminating valley to another one in the neighborhood. Along this part the GE curve reduces the energy in comparison to the former part (this is the characterization of a turning point of a GE). The hysteresis of curves 1 (uphill) and 2 (downhill) disturbs the unique definition of the reaction pathway, and, of course, also the applicability of theories which are based on the reaction path definition. This is due to the shape of the PES. It is an intrinsic problem and cannot be solved by mathematical tricks. Also the lines of steepest descent from the SP flow asymptotically into the valley floor of the lower "reaction path" which starts from the minimum. It is impossible to determine the "point of confluence" of the two lines by a local criterion [4]. Note, turning points are frequent already on the PES of the simple four-atom molecule formaldehyde, H_2CO [27].

The behavior of the TASC at the "side-on"-type turning points described with the help of Fig. 3 is typical for most turning point situations which we met in our tests; however, there are also tests where the search, using corrector steps, finds a ridge GE without crossing the SP. If this happens, we go down the ridge and find the SP as well.

3.3 The bifurcation of a streambed GE

The so-called Don Quixote SP [18] has a decomposition mode larger in its absolute value than at least one of the residual ridge modes. An example is shown in Fig. 4 modeling a unimolecular reaction step

$$E(x,y,z) = x^2\left(80 - y^2\right)^2/80 + 0.2x^4 + 0.1y^2\left(200 - y^2\right) + 100z^2, \tag{14}$$

where the section $z = 0$ is drawn. (The z coordinate may simulate the $(n - 2)$ remaining coordinates of a molecule; it is only symbolically given by a strong pure harmonic term.) The potential partly imitates the rotation and inversion processes of $CH_2NO_2^-$ treated in Ref. [28]. The PES (Eq. 14) has one minimum at (0, 0, 0) and two SPs at (0, ± 10, 0). To avoid the pure symmetric pathway, we started the TASC at (0.01, 0.1, 0.0) near the minimum in the positive y direction along curve 1, which is the eigenvector and gradient direction of the "uphill streambed" GE to the smallest (absolute) eigenvalue. The TASC jumps over the GE bifurcation point [29] at $y = 5.2$ and also over the inflection point of the corresponding energy profile at $y = 5.8$ (not visible in the figure). At the y-axis, the second eigenvector points in the x direction controlled by symmetry. At $y = 7.2$ the region of the Don Quixote SP begins where the eigenvalue of the x direction becomes smaller than the absolute value of the negative eigenvalue along the y-axis GE. The streambed GE along the y-axis (curve 1 and a part of curve 2 both calculable using the TASC)

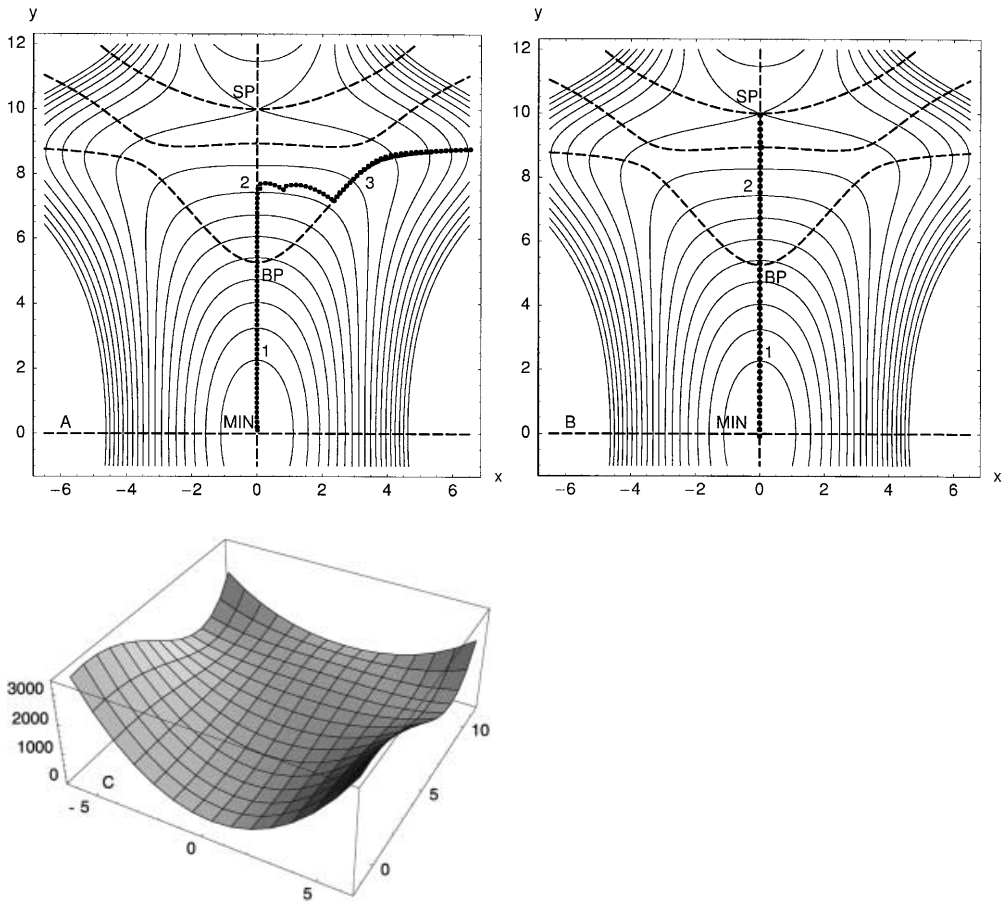

Fig. 4A–C. Model potential surface, $E(x, y, 0) = x^2(80 - y^2)^2/80 + 0.2x^4 + 0.1y^2(200 - y^2)$, with a MIN and a SP. Analytically calculated GEs are shown by *bold dashed lines*; they bifurcate at bifurcation points (*BP*) **A** The tangent search (TASC, *dotted curve*) explores the streambed GE using a fixed predictor step length of 0.15 and a corrector tolerance of 0.00005. The corrector step length is that of a Newton–Raphson step which is restricted to the predictor step length if necessary. The TASC starts at the MIN but does not directly meet the Don Quixote SP along the y-axis because this SP is not situated on top of the streambed. **B** The SP is available using a combination of the TASC with the original RGF method which is switched on at the crossing of the eigenvalues along pathway 2, see text. **C** View over the surface

"ends" at $y \approx 7.1$. The predictor becomes unstable and after two steps, the corrector breaks out. The procedure finds the new streambed, GE3, as one of two GE side branches. This GE3 goes uphill to infinity. Thus, in such a particular case, the tangent search method cannot find the SP on the y-axis because this SP is not connected with the minimum by a usual streambed. In contrast, the branches of the bifurcated reaction path, GE3, have lower slopes than the further GE following the y-axis (GE2). The region of GE2 after the breakout of the TASC is a cirque. The bifurcation point [14, 29] of the y-axis GE at 5.2 does not disturb the TASC because the TASC depends only on the eigenvalues of the Hessian, but the GE bifurcation is additionally influenced by the values of the gradient and the third derivatives of the potential. (The example shows that the bifurcation of a GE generally does not take place at the crossing point of the eigenvalues. This contrasts with a remark in Ref. [17].)

When looking at the whole PES the y-axis GE (1 and 2 in Fig. 4) is shown to be the pathway connecting the global minimum and the SP. Of course, this is exactly the steepest descent from the SP, the IRC. It coincides with the y-axis GE; however, the IRC only works downhill. How can a global working procedure be defined? There are two strategies. The first would mean to follow only the streambed, i.e., the TASC. As shown in Fig. 4A, the bifurcation of the y-axis GE (calculable with the GE theory [29]) leads to two branches of weaker slope. By definition, these branches are the streambeds; however, these streambed GEs avoid the SP on the y-axis. The second strategy is also to follow the streambed uphill to its end as in Fig. 4A, but in addition to try to find a possible SP in the previous streambed direction after the eigenvalue-crossing. This cannot be done by the TASC. We simply use a link to the original RGF. Because the second (positive) eigenvalue, λ_2, becomes lower than $|\lambda_1|$ after the crossing, the shape of the PES can be compared with a broad "waterfall", but it does not fulfill the definition of a streambed, where flows from the left-hand side and from the right-hand side would be confluent. The valley along the y-axis GE through the SP in the direction of the decomposition mode still continues to be a valley, but a special kind of it, a so-called cirque. Steepest descent lines in this region do not flow into each other in a "singular steepest descent" line [17], which may be the usual line of the MEP concept. Steepest descent lines starting in the neighborhood of the Don Quixote SP go downhill in a nearly parallel manner. Thus, the method used should not be enforced to find exactly one defined MEP. At the "breakout point" of the TASC, it is sufficient to go further uphill to the Don Quixote SP using the original RGF method following any (fixed) gradient direction of the "waterfall". This is demonstrated in Fig. 4B. The pathway uphill from the minimum to the end of the streambed is given by the TASC. However, at $0.9\lambda_2 < |\lambda_1|$ the procedure jumps to the RGF under the fixed search direction of the gradient

of the last TASC step. Note that the deviation is not visible in Fig. 4B. The maximal deviation from the pathway of curve 2 is reached at (0.031, 8.947). After this point the RGF procedure converges quickly back to the saddle point at (0,10).

3.4 Examples: search for SPs of LJ clusters along their streambed GE

The potential of the proposed method is best appreciated when it is applied to systems with an analytic potential which is computationally inexpensive to evaluate. Argon clusters provide excellent examples of such systems where the intracluster interactions are well described by simple pairwise additive terms. We use the LJ potential [30] for the $3N$-dimensional cluster of N argon atoms. The energy of the LJ_N cluster is given by the pairwise additive function

$$E_N = 4\varepsilon \sum_{i=1}^{N-1} \sum_{j=i+1}^{N} \left[\left(\frac{\sigma}{r_{ij}}\right)^{12} - \left(\frac{\sigma}{r_{ij}}\right)^{6} \right] , \qquad (15)$$

where ε is the pair potential well depth, $\sigma = 0.3405$ nm is the separation appropriate for argon where the pair interaction goes through zero, and r_{ij} is the separation of atoms i and j. The energy is given in LJ reduced units: $\varepsilon = 1.671 \times 10^{-14}$ erg. A Fortran program for the LJ potential developed by D.J. Wales is used.

We will confirm on the LJ clusters that the "uphill streambed" GE does not necessarily lead to the next SP (see Sect. 3.3 and earlier work [4]). Our search for a "streambed" SP of an isomerization path of LJ_N starts at minima which have been well cataloged in the Cambridge Cluster Database [31]. We reduce the $3N$ Cartesian coordinates to $n = (3N - 6)$ internal coordinates referring to the z-matrix output of the program MOLDEN [32]. $(N - 1)$ distances, $(N - 2)$ angles, and $(N - 3)$ dihedrals are used. The start direction of the TASC is the eigenvector to the smallest eigenvalue (or any approximation), where both signs of the direction are probed. We found the SPs given in Table 1. Every SP was refined by a Newton–Raphson run and, additionally, a steepest descent test was done to check its connection to the initial minimum. Because we are interested in the streambed GEs, the step length of the predictor used by the TASC in the first run is kept small. The number of predictor and corrector steps given in Table 1 is obtained from tests for fixed maximal step lengths, for which the algorithm still works. For example, to get the result for LJ_{20} in Table 1, eight predictor steps and 17 corrector steps are necessary using the predictor step length of 0.5 and a corrector threshold of 0.1. We need 34 predictor steps and 23 corrector steps for the step length 0.2 for the predictor and the corrector threshold of 0.01. If the step length is reduced to 0.07, we have 95 predictor steps but only 17 corrector steps to reach the SP. (A too large step length may result in a distant starting point for the corrector which may diverge, or the steps for internal coordinates are too large and/or the z-matrix does not work.) Note that the TASC program used is still a development version; no attempt was made at performance optimization.

To somehow illustrate the higher-dimensional cases of an LJ cluster, we give a picture of the simple three-atomic, three-dimensional case [33] of LJ_3 in Fig. 5. The Cartesian plane of the pathway of the third argon atom is shown when moving around the first two argon atoms which are fixed on the x-axis. The TASC pathway climbs up along the very flat valley-floor GE, but the surface along orthogonal directions to the pathway of LJ_3 shows very strong curvatures. The contrast of the curvatures is a general feature of the LJ_N potential.

The SPs found using the TASC for LJ_7 and LJ_8 agree with the structures given in Refs. [15, 34, 35]. These SPs are points on top of the streambeds which connect the SP and the minimum from which the search was started. As expected, we are able to find the corresponding "floor lines" of isomerization paths of these clusters.

For LJ_{15}, we can find a much lower SP (Table 2) than the SP found as a putative lowest SP in Ref. [35]. The reason may be due to particularities of the PES around the SP. The pathway over the SP is extremely flat along the decomposition mode, but the curvature of most of the orthogonal directions is large. It forms a SP with cross-sections of extreme curvature. Such a very narrow defile in the energy mountains will represent a small reactive volume in the configuration space, and it may be difficult to find the pathway using the stochastic algorithms used in Ref. [35]. However, this SP of LJ_{15} is not found by using the TASC alone. Up to $-50.6\ \varepsilon$ the valley profile uphill shows a large negative curvature like a stair, followed by the terraced SP region. The TASC search breaks out as in Fig. 4A. It does not find the SP region and it climbs further uphill by a large number of corrector steps. However, as in Fig. 4B, the SP is finally reached by the combination with the RGF method, which we switch on if the eigenvalue $0.9\ \lambda_2$ is lower than $|\lambda_1|$. The search direction of the RGF is fixed to the last ascent direction before the crossing.

The low SP found in the LJ_{20} cluster is also of some interest (Table 3). Again, the SP is not found by the pure TASC going up the streambed. At $-75.12\ \varepsilon$ the first two eigenvalues cross. $|\lambda_1|$ becomes greater than λ_2. Using corrector steps, after the crossing the TASC goes around the SP and finds a ridge GE. Turning down the search there, we find the desired SP along this detour. Thus, the resulting pathway is not a GE to the smallest eigenvalue throughout. Using the second strategy, on the other hand, the TASC is switched onto the RGF method at the eigenvalue crossing as in Fig. 4B. The result is a cirque GE. Additionally, the second eigenvalue becomes negative at $-74.91\ \varepsilon$; thus, a valley-ridge inflection point [6, 9] is met. The RGF method overcomes this difficulty by following a bluff and then finding the SP. (The finding of valley-ridge inflection points of the PES [6, 9] is out of range of the tangent search method because there the "second" eigenvalue moves through zero, by definition; thus, it is smaller than the eigenvalue in the path direction.)

The decomposition modes of the SPs of some other clusters are also very small. For $N \geq 13$, the ratio $|\lambda_1|{:}\lambda_n$ is of the order of 1:200. Some SPs are extreme "Sancho Panza" type SPs [18] (flat saddle passage, narrow valley like a short, fat donkey). LJ_{20} and LJ_{55} are exceptions, as

Table 1. Ar_N cluster energies (in ε units) for global minima and the saddle points which are connected by the tangent search concept (*TASC*) or by TASC and the reduced gradient following, with fixed predictor step length; and the first, second, and last eigenvalue at the saddle points (*SP*). *Last row*: number of predictor and corrector steps ($P + C$). N is the cluster size and n is the dimension of the configuration space

N	n	E(Min)	E(SP)	EV_1	EV_2	EV_n	P + C
3	3	−3.000	−2.031[a]	−0.0198	5.038	15.245	2 + 3
7	15	−16.505	−15.444[a]	−0.8654	2.728	21.003	8 + 12
8	18	−19.821	−18.806[a] (−19.281[b])	−0.8198	1.428	24.553	11 + 10
15	39	−52.322	−50.528 (−50.239[c] −48.798[d])	−0.2279	0.4580	48.502	14 + 23
20	54	−77.177	−74.991	−0.5429	0.5928	69.230	8 + 17
30	84	−128.286	−125.595	−0.4803	0.1639	83.395	21 + 28
55	159	−279.248	−270.616[a] (−276.239[e])	−0.3582	0.9490	72.278	15 + 31

[a] The SP is arrived at using the TASC; thus, it is on top of a valley gradient extremal
[b] There is a lower-energy SP of first order [34] which is inaccessible by a streambed gradient extremal from the global minimum
[c] A higher-energy SP of first order reached in this work by a jump between two streambed gradient extremal, as in Fig. 4
[d] There is a much higher SP of first order [35] which is inaccessible using a streambed gradient extremal from the global minimum
[e] A number of lower-energy SPs of first order [34, 39] are inaccessible using a streambed GE from the global minimum

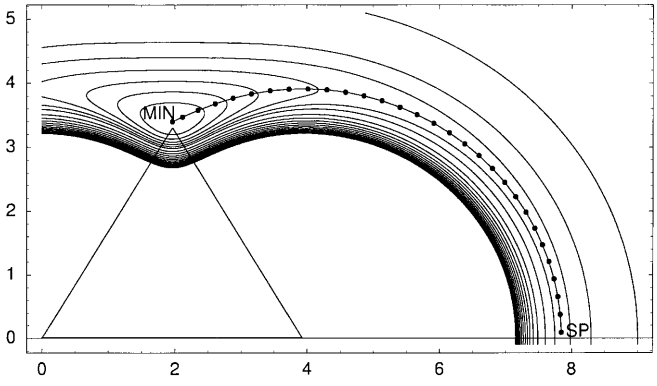

Fig. 5. Lennard-Jones potential of Ar_3. The Cartesian plane shows the movement of the third Ar atom around the first two Ar atoms which are fixed at zero and at the x-axis. The equilibrium structure is the equilateral triangle and the SP is a linear structure on the x-axis. The TASC pathway (*dotted curve*) climbs up along the valley-floor GE using a fixed predictor step length of 0.0725 and a corrector tolerance of 0.0025

Table 2. Geometry of the lowest SP at -50.528ε for the system of the Ar_{15} cluster

Atom	x	y	z
1	−0.04836158	0.01647163	−0.06104223
2	−0.04836158	0.01647163	3.73082246
3	3.60173663	0.01647166	−0.38034045
4	1.74049195	3.42338288	−0.87607992
5	0.67786044	−3.15920862	1.70025666
6	−2.14270393	−3.26090370	−0.75417290
7	−1.63119227	2.73733305	−2.22527963
8	2.51979433	2.32677921	2.50659959
9	3.50802030	−1.23196075	3.17422691
10	1.39404502	−2.71923000	−2.06340965
11	1.55010075	0.79716210	−3.47927384
12	−1.25743824	3.01150870	1.60976057
13	−2.91083623	−1.98424934	2.62349887
14	−1.79466583	−0.79329827	−3.43488469
15	−3.70764219	0.30912110	−0.23941487

Table 3. Geometry of the lowest saddle point at -74.991ε for the system of the Ar_{20} cluster

Atom	x	y	z
1	0.4586277119	1.7563789205	0.1662820679
2	0.4586277119	1.7563789205	3.7650045973
3	3.8527506190	1.7563789205	1.6380240637
4	1.8492530016	4.9482412859	1.3367993440
5	−0.2392746122	4.7197919716	−1.9431628950
6	2.9671610982	−0.5594993359	−1.3430095533
7	−0.5065121994	−1.6168138191	−0.2812529827
8	2.0861704149	−1.4783390886	2.2545212094
9	−1.1821699055	−1.7433867937	4.0474010268
10	−2.7467658067	0.6428282338	1.7957924784
11	−2.9245108676	−1.4709518059	−2.9774908085
12	0.6978557504	−2.6218315614	−3.6986210691
13	−0.4000866318	−4.6670039459	1.9439079944
14	−2.8878274128	2.0574036788	−1.5840744608
15	2.2290293989	−4.1663325028	−0.6206086564
16	−1.8760808119	4.2727638451	1.5183921321
17	−3.6795311179	−2.9331394592	0.9358728746
18	0.2022972739	1.0554040646	−3.4094421217
19	3.1957007644	3.1686503774	−1.8830023717
20	−1.5547143792	−4.8769219064	−1.6613328696

can be seen from the first two eigenvalues. The eigenvalues of the decomposition mode, the weakest as well as the strongest mode, λ_n, of the cluster treated, are reported in Table 1. It appears that the LJ potential of Eq. (15) seems to be an extreme energy hypersurface, making these systems excellent test cases for the proposed method.

The SP structure found for LJ_{30} is given in Table 4. The SP has the type described in Sect. 3.3: the first two eigenvalues form the characteristic of a Don Quixote SP. It is not available through following the TASC, but through the mixed strategy described earlier. It is presumed (cf. Fig. 4B) that this leads to the next SP if it exists at all. For the SP of LJ_{30}, the algorithm changes twice between the TASC and the RGF. At $-126.5\ \varepsilon$ and $-125.6\ \varepsilon$, it jumps from following the tangent search to the RGF, but in-between, after going down with corrector steps, it comes back to the TASC at $-126.7\ \varepsilon$. In

Table 4. Geometry of the SP at -125.595ε for the system of the Ar_{30} cluster

Atom	x	y	z
1	−2.0970363983	−0.7892923341	−4.6033067148
2	−2.0970363983	−0.7892923341	−0.9286209663
3	1.5360422712	−0.7892923341	−5.0534884628
4	4.8937241689	−0.5521820671	−3.5949563424
5	4.3201561746	0.8635847015	−0.1854306611
6	3.2525083734	−2.1040052411	2.1264239994
7	−0.4045022381	−2.9818556065	1.5149700938
8	−0.6783333182	−3.8358914622	−2.6322292430
9	−4.3325876349	−2.7167590444	1.3456800682
10	−5.0530223459	1.1161904345	0.3806790499
11	−1.7365545942	3.0542231207	0.3986852480
12	−3.2180138859	2.3517496086	−2.9084270245
13	−0.2959670303	4.9832492483	−2.6401262228
14	0.3537063498	1.4274138920	−2.2947327017
15	1.9947213713	3.8556851445	0.2353911439
16	−0.1294564902	2.8986630501	3.8211363867
17	0.6740067143	−0.8167927164	4.6206577463
18	−2.6019550049	−2.8174658000	4.7718392368
19	−2.3130972529	0.0940615627	2.5991108709
20	−3.9910448902	3.2171720076	3.4883271434
21	−5.6020126603	−0.2849799133	4.0813685412
22	−2.4634188091	0.8386338999	6.1625267502
23	−0.3982471958	2.5341627977	−5.6670273023
24	3.4229760729	2.9796997987	−3.3248753969
25	3.4778416398	1.6216839205	3.4506279780
26	0.8740745632	0.5240233418	1.1661391534
27	3.1289100139	−4.0860988997	−3.8591505775
28	1.9401169315	−1.6683975067	−1.4174650752
29	2.1914604745	−5.1151829656	−0.2231704596
30	5.3520410283	−3.0127083037	−0.8305562593

this manner, the SP region is reached but the SP again is only available using the RGF.

$N = 55$ is a magic number for an Ar_N cluster, because its global minimum structure represents the closure of the second shell of atoms in an icosahedral packing geometry [36]. For this, the largest cluster treated in this work simulated by LJ_{55}, we found the SP at -270.60ε using the TASC, which lies very high in the mountains of the PES [23, 24, 34, 37]. We obtained it on top of a streambed GE using the TASC. The cluster has a so-called sawtooth potential [38]. Additionally, it is known that LJ_{55} has a number of further low-lying SPs which connect minima but do not include the global one [23]. It becomes clear from the corresponding disconnectivity graph [39] that these SPs of first order should be inaccessible using the streambed GE from the global minimum, however, other SPs as well [40, 41], which are connected to the global minimum, forming the sawteeth of the main bowl of the PES are not reached by the tangent search uphill. They belong to normal-mode directions of larger eigenvalues of the minimum. Thus, they are located at the side slopes of the streambed GE.

4 Conclusion

We demonstrated the workability of the new algorithm, TASC, for following the streambed GE as exactly as we need it, including the SP of first order lying on the top of the streambed GE. We started at a given minimum in the direction of the "smallest" eigenvector, but we did not use any further external knowledge to continue, like many salmon swimming upstream. (Alternatively, we may also start at a SP and go down. In the case of a continual streambed this leads to the same line!) We only need the evaluation of the gradient and the Hessian per step. Examples are an ab initio model potential for H_2O as well as an LJ custer containing up to 55 atoms. The TASC is a modified RGF method comparable in its effort with the RGF method [5, 6, 9]. Only the projector matrix, $P_{x'(t)}$, now has to be recalculated for Eq. (2) after every predictor step. The additional numeric effort is next to nothing. The new procedure is a potent method for studying the streambeds of multidimensional surfaces. Its success is based on the numerical tracing of the MEP, which we mathematically understand as the valley-floor GE. This success results from the self-correction of the modified RGF method: The tangents of the RGF solutions to different directions are "contractive" in the sense that they are always a "better" guess than a constant RGF direction to search for the streambed line. The original RGF [5, 6] already forms an effective tool to find SPs where the choice of the search direction is quite arbitrary; however, the RGF can diverge more or less from the MEP even if it starts in the eigenvector direction. The choice of the actual tangent in the TASC now overcomes (and restricts) the arbitrariness of the choice of direction used in the RGF method. The solution of the TASC is, after some initial iterations, uniquely defined by the PES, actually a numeric approximation of the valley-floor gradient extremal. However, this is also its "fault": its special mathematical working mechanism restricts the TASC to only GE pathways where the valley direction represents the smallest (absolute) eigenvalue. The overwhelming complexity of all possible GEs (Fig. 4A) is automatically ruled out by the TASC to the one valley-floor GE, which is that GE which is frequently of primary chemical interest. For instance, the method should be suitable to follow proton (or substituent) migrations in protonated systems, for example, in protonated olefins and aromatic compounds, cf., for instance, the proton motion in protonated benzenes and ethylenes [42]. Researchers often wish to find the streambed in the conformational space of dihedral angles which represent the weakest modes in a molecule [43]. For example, in the currently discussed folding–unfolding problem of proteins, it is assumed that weak dihedral variables are mainly involved [44].

The special SP-type of so-called Don Quixote characteristics is not situated on the top of a streambed. It is not attainable using the TASC alone but by combination with the RGF method. So some very flat SP defiles of an LJ cluster lying in extremely narrow valleys are quickly found. Further, bifurcation points of the streambed GE are not necessarily indicated by the TASC, but the crossing of the absolute values of the first two eigenvalues disturbs the search and forces the corrector to search (by controlled step length) for another streambed GE in the "neighborhood". Again it appears that the

limitation of the TASC can be overcome by the combination with the original RGF method.

Acknowledgements. Our work was made possible through the financial support of the Deutsche Forschungsgemeinschaft as well as through the help offered by the Naturwissenschaftlich-Theoretisches Zentrum der Universität Leipzig.

Appendix

1 Scheme of the TASC algorithm

1. Initialisation, preparing and execution of first step along given direction.
2. Transform internal to Cartesian coordinates.
   Calculate energy, gradient, and Hessian matrix.
   Mass weighting.
   Calculate metric tensor, g, and coordinate transformation, B.
   Transform gradient and Hessian into internal coordinates [16].
   Vibrational analysis [9].
   Calculate Newton–Raphson step for STOP criterion 6.
   Project gradient and Hessian by tangent projector of last predictor.
   Calculate new tangent by QR decomposition.
3. Test of tolerance

Predictor	Corrector
Calculate step length [45]. Calculate step along new tangent.	Solve Eq. (2) by steps orthogonal to search direction [46].

4. Optional: test of smallest eigenvalues, λ_i

Continue TASC (up or down) by	Jump to RGF [5, 6]:
last tangent: $=\pm$(new tangent).	hold search direction.

5. Store actual values, and execute the step.
6. Repeat steps 2–5 until STOP criterion is satisfied: the stationary point is found.

2 Proof that the TASC yields a gradient extremal

For simplicity, we only treat the two-dimensional case. Instead of the RGF we may use the equivalent Branin method, Eq. (6). There is the tangent, $\mathbf{x}'$, of a solution of the RGF, as well. The projector of the original RGF was $\mathbf{P_r}$ to the search direction, $\mathbf{r}$. We replace this constant direction after every predictor step by the direction of the tangent, $\mathbf{x}'$. Thus, the projector for the next step must be constructed with the vector $\mathbf{Ag}$. If the Hessian is

$$\mathbf{H} = \begin{pmatrix} h_{11} & h_{12} \\ h_{12} & h_{22} \end{pmatrix} , \tag{A1}$$

then

$$\mathbf{A} = \begin{pmatrix} h_{22} & -h_{12} \\ -h_{12} & h_{11} \end{pmatrix} \tag{A2}$$

because

$$\mathbf{HA} = \begin{pmatrix} h_{11}h_{22} - h_{12}^2 & 0 \\ 0 & h_{11}h_{22} - h_{12}^2 \end{pmatrix} = \det(\mathbf{H})\mathbf{I} . \tag{A3}$$

Now

$$\mathbf{Ag} = \begin{pmatrix} h_{22}g_x - h_{12}g_y \\ -h_{12}g_x + h_{11}g_y \end{pmatrix} \tag{A4}$$

and

$$\mathbf{P_{Ag}} = (\mathbf{Ag})^{\perp} = \left(h_{12}g_x - h_{11}g_y, h_{22}g_x - h_{12}g_y\right) . \tag{A5}$$

If we search for a solution curve of Eq. (2) this becomes

$$\mathbf{P_{Ag}g} = 0 . \tag{A6}$$

We get

$$h_{12}\left(g_x^2 - g_y^2\right) + (h_{22} - h_{11})g_x g_y = 0 , \tag{A7}$$

which is the equation of the gradient extremal [11].

References

1. Laidler K (1969) Theory of reaction rates. McGraw-Hill, New York
2. (a) Miller W, Handy NC, Adams JE (1980) J Chem Phys 72: 99; (b) Billing GD, Mikkelsen KV (1997) Advanced molecular dynamics and chemical kinetics. Wiley, New York
3. Truhlar DG (1995) In: Heidrich D (ed) The reaction path in chemistry: current approaches and perspectives. Kluwer, Dordrecht, p 229
4. Quapp W, Heidrich D (1984) Theor Chim Acta 66: 245
5. Quapp W, Hirsch M, Imig O, Heidrich D (1998) J Comput Chem 19: 1087
6. Quapp W, Hirsch M, Heidrich D (1998) Theor Chem Acc 100: 285
7. (a) Truhlar DG, Garrett BC (1980) Acc Chem Res 13: 440; (b) Isaacson AD (1995) In: Heidrich D (ed) The reaction path in chemistry: current approaches and perspectives. Kluwer, Dordrecht, p 191
8. (a) Baboul AG, Schlegel HB (1997) J Chem Phys 107: 9413; (b) Eckert E, Werner HJ (1998) Theor Chem Acc 100: 21
9. Hirsch M, Quapp W, Heidrich D (1999) Phys Chem Chem Phys 1: 5291
10. (a) Basilevsky MV, Shamov AG (1981) Chem Phys 60: 337; (b) Basilevsky MV, Shamov AG (1981) Chem Phys 60: 347
11. Hoffman DK, Nord RS, Ruedenberg K (1986) Theor Chim Acta 69: 265
12. (a) Jørgensen P, Jensen HJA, Helgaker T (1988) Theor Chim Acta 73: 55; (b) Quapp W (1989) Theor Chim Acta 75: 447
13. Sun JQ, Ruedenberg K (1993) J Chem Phys 98: 9707
14. Heidrich D, Kliesch W, Quapp W (1991) Properties of chemically interesting potential energy surfaces. Lecture notes in chemistry 56. Springer, Berlin Heidelberg New York
15. Jensen F (1995) J Chem Phys 102: 6706
16. Quapp W (1995) In: Heidrich D (ed) The reaction path in chemistry: current approaches and perspectives. Kluwer, Dordrecht, p 95
17. Ruedenberg K, Sun JQ (1994) J Chem Phys 100: 5836
18. Mezey PG (1987) Potential energy hypersurfaces. Elsevier, Amsterdam
19. Guest MF, Fantucci P, Harrison RJ, Kendric J, van Lenthe JH, Schoeffel K, Sherwood P (1993) GAMESS-UK program. CFS, Daresbury Laboratory
20. Branin FH (1972) IBM J Res Dev 504
21. Turner AJ, Moliner V, Williams IH (1999) Phys Chem Chem Phys 1: 1323
22. Cerjan CJ, Miller WH (1981) J Chem Phys 75: 2800
23. Wales DJ (1993) J Chem Soc Faraday Trans 89: 1305
24. Wales DJ (1994) J Chem Phys 101: 3750
25. Quapp W, Imig O, Heidrich D (1995) In: Heidrich D (ed) The reaction path in chemistry: current approaches and perspectives. Kluwer, Dordrecht, p 137
26. Perkovic S, Blokhuis EM, Han G (1995) J Chem Phys 102: 400
27. Jensen F (1998) Theor Chem Acc 99: 295
28. Mezey PG, Kresge AJ, Csizmadia IG (1976) Can J Chem 54: 2526
29. Basilevsky MV (1987) Theor Chim Acta 72: 63
30. Lennard-Jones JE (1924) Proc R Soc Lond Ser A 106: 463

31. Wales DJ, Doye JPK, Dullweber A, Naumkin FY The Cambridge cluster database URL http://brian.ch.cam.ac.uk/CCD.html
32. Schafternaar G MOLDEN. CAOS/CAMM Center Nijmegen Toernooiveld, Nijmegen, The Nethelands
33. Hinde RJ, Berry RS, Wales DJ (1992) J Chem Phys 96: 1376
34. Doye JPK, Wales DJ (1995) J Chem Phys 102: 9673
35. Chaudhury P, Bhattacharyya SP, Quapp W (2000) Chem Phys 253: 295
36. (a) Hoare MR (1979) Adv Chem Phys 40: 49; (b) Harris IA, Kidwell RS, Northby JA (1984) Phys Rev Lett 53: 2390
37. Wales DJ, Doye JPK (1996) In: Martin TP (ed) Large clusters of atoms and molecules. Kluwer, Dordrecht, p 241
38. (a) Ball KD, Berry RS, Kunz RE, Li FY, Proykova A, Wales DJ (1996) Science 271: 963; (b) Vekhter B, Berry RS (1997) J Chem Phys 106: 6456
39. Doye JPK, Miller MA, Wales DJ (1999) J Chem Phys 111: 8417
40. Wales DJ (1990) Chem Phys Lett 166: 419
41. Uppenbrink J, Wales DJ (1992) Chem Phys Lett 190: 447
42. (a) Heidrich D, Grimmer M (1975) Int J Quantum Chem 9: 923; (b) Olah GA, Schlosberg RH, Porter RD, Mo YK, Kelly DP, Mateescu GD (1972) J Am Chem Soc 94: 2034; (c) Heidrich D, Grimmer M, Köhler HJ (1976) Tetrahedron 32: 1139; (d) Heidrich D, Grimmer M, Köhler HJ (1976) Tetrahedron 2027; (e) Köhler HJ, Heidrich D, Lischka H (1977) Z Chem 17: 67
43. (a) Santana LN, Suvire FD, Enriz RD, Torday LL, Csizmadia IG (1999) J Mol Struct (THEOCHEM) 465: 33; (b) Kolossváry I, Guida WC (1999) J Comput Chem 20: 1671; (c) Ben-Avraham D, Tirion MM (1998) Physica A 249: 415; (d) Gotō H, Ósawa E (1993) J Mol Struct (THEOCHEM) 285: 157
44. (a) Gruebele M (1999) Annu Rev Phys Chem 50: 485; (b) Černohorský M, Kottou S, Koča J (1999) J Chem Inf Comput Sci 39: 705; (c) Durup J (1998) J Mol Struct (THEOCHEM) 424: 157; (d) Hansen A, Jensen MH, Sneppen K, Zocchi G (1998) Physica A 250: 355; (e) Chen YZ, Mohan V, Griffey RH (1998) Phys Rev E 58: 909; (f) Lazarides T, Karplus M (1997) Science 278: 1928; (g) Argos P, Abagyan R (1994) Comput Chem 18: 225; (h) Rackowsky S, Scheraga HA (1984) Acc Chem Res 17: 209
45. (a) Schlick T (1992) In: Lipkowitz KB, Boyd B (eds) Reviews in computational chemistry, vol III. VCH, New York, p 1; (b) The Computational Science Education Project (1995) Mathematical optimization, http://csep1.phy.ornl.gov/CSEP/MO/NODE11B.html
46. Allgower EL, Georg K (1990) Numerical continuation methods – an introduction. Springer, Berlin Heidelberg New York